Expansion of ferromagnetism by calcium doping in the ordered oxygen deficient perovskite $EuBaCo_2O_{5.50 \pm \delta}$



2008 J. Phys.: Condens. Matter 20 015212

(http://iopscience.iop.org/0953-8984/20/1/015212)

J. Phys.: Condens. Matter **20** (2008) 015212 (7pp) doi:10.1088/0953-8984/20/01/015212

# Expansion of ferromagnetism by calcium doping in the ordered oxygen deficient perovskite $EuBaCo_2O_{5.50\pm\delta}$

**Md Motin Seikh**[1], **V Caignaert, V Pralong, Ch Simon and B Raveau**[2]

CRISMAT, ENSICAEN-CNRS UMR 6508, 6 Boulevard Maréchal Juin, 14050 Caen, France

E-mail: bernard.raveau@ensicaen.fr

Received 28 August 2007, in final form 30 October 2007
Published 5 December 2007
Online at stacks.iop.org/JPhysCM/20/015212

**Abstract**

The effect of calcium doping on the magnetic and transport properties of $Eu_{1-x}Ca_xBaCo_2O_{5.50\pm\delta}$ has been investigated for $x \leqslant 0.2$. The substitution of calcium for europium does not change the cobalt valency, which remains +3, due to a small oxygen deficiency with respect to the ideal '$O_{5.5}$' composition. This substitution induces a large expansion of the ferromagnetic state in the whole temperature range from 10 to 320 K, $T_C$ increasing with the calcium content. Moreover, we observe a substantial decrease of the effective moment in the paramagnetic phase as $x$ increases. In contrast, the Ca-doping does not significantly affect the metal–insulator transition. However, the resistivity and magnetoresistance decrease drastically for a small doping rate. These results are explained by a new scenario where we consider the presence of canted antiferromagnetic domains and a disproportionation mechanism of the cobalt $Co^{3+}$ into $Co^{2+}$ and $Co^{4+}$.

(Some figures in this article are in colour only in the electronic version)

## 1. Introduction

Transition metal oxides with the perovskite structure exhibit a wide range of fascinating physical properties due to the strong interplay between spin, charge, orbital and lattice degrees of freedom. However, the cobaltites display an additional parameter, namely spin-state transition which throws an extra challenge to understanding magnetism in cobalt oxides. Like other transition metal oxides, cobaltite can accommodate oxygen vacancies giving rise to variable ratios of $Co^{2+}$, $Co^{3+}$ and $Co^{4+}$, each with three possible spin states: the low-spin (LS) state, the intermediate-spin (IS) state and the high-spin (HS) state, which have a strong influence on the electrical and magnetic properties of the system. Such spin states originate from a close competition between the atomic parameter Hund's exchange energy and the crystal field energy. Thus, a small variation in structural parameters, temperature, pressure or magnetic field can produce a drastic change in the physical properties.

The ordered oxygen deficient perovskites, with the ideal formula $LnBaCo_2O_{5.50}$, have been a topic of numerous investigations, due to their fascinating magnetic and magnetotransport properties [1–18]. The structural degree of freedom of this family of compounds provides a strong playground to explore the interrelation between electronic, magnetic and structural properties. The crystal structure of these oxides can be described as an ordered oxygen deficient perovskite (figure 1), where 1:1 ordering of the $Ba^{2+}$ and $Ln^{3+}$ layers implies the formation of layers of $CoO_6$ octahedra interconnected by rows of $CoO_5$ pyramids. Such a structure is very flexible, i.e. sensitive to tiny variations of the oxygen content and to the size of the $Ln^{3+}$ cation, so that long range order superstructure or even local distortions can be obtained, leading to dramatic variations of the magnetic properties [10, 17, 19, 20] from one sample to the other.

Besides the existence of magnetoresistance and of room temperature metal–insulator transition ($T_{IM}$) [1–3], these cobaltites exhibit an intriguing magnetic behaviour, involving the appearance of a ferromagnetic moment in a rather narrow temperature window, i.e. for ∼200 to ∼300 K. The interpretation of the latter phenomenon

[1] Present address: Department of Chemistry, Visva-Bharati University, Santiniketan-731235, West Bengal, India.

[2] Author to whom any correspondence should be addressed.

 

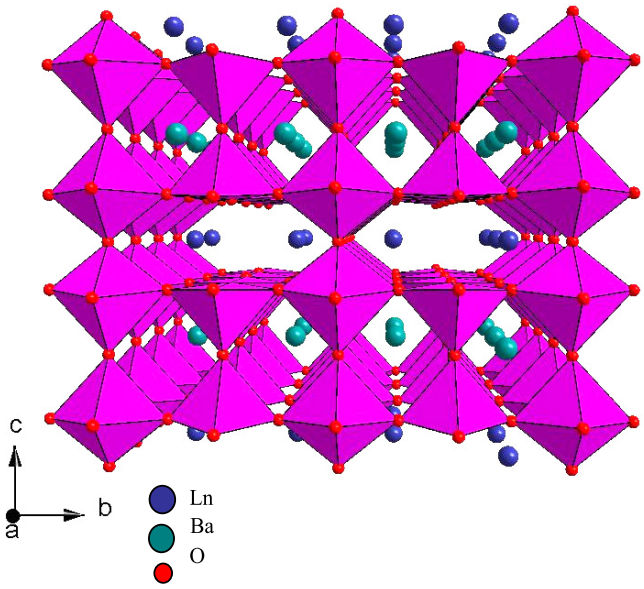


**Figure 1.** Structure of $LnBaCo_2O_{5.50}$ with layers of $CoO_6$ octahedra interconnected with rows of $CoO_5$ pyramids indicating the doubling of unit cell along the *b* and *c* axes.

is rather controversial, as shown from the study carried out by Taskin *et al* [6] for the Gd phase and by Plakhty *et al* [18] for Tb phase. The former authors propose a mechanism involving successive paramagnetic–ferromagnetic–antiferromagnetic (PM–FM–AF) transitions based on a magnetic structure built up of $S = 1$ $Co^{3+}$ cations separated by non-magnetic $S = 0$ $Co^{3+}$ cations, whereas the latter proposed a ferrimagnetic structure at 260 K and two antiferromagnetic structures at 230 K and 100 K, respectively. Many researchers take support of the spin-state transition mechanism to explain the magnetic data and the metal–insulator transition. The presence of LS $Co^{3+}$ ion ($S = 0$), should be in a perfectly octahedral site. However, an orthorhombic or a tetragonal distortion will destabilize the $S = 0$ state, due to the gain in crystal field energy and lower electron–electron repulsion. There are also both experimental and theoretical reports which disagree with the occurrence of spin-state transitions in this system across the $T_{IM}$ [21–25].

These controversial reports clearly demonstrate that an understanding of the nature of magnetic and electrical transitions in these cobaltites is far away. Here we report the effect of the substitution of calcium for europium upon the magnetic and electrical properties of $EuBaCo_2O_{5.50\pm\delta}$. Interestingly, by the substitution of trivalent $Eu^{3+}$ with divalent $Ca^{2+}$ the average cobalt valence remains ∼3+ at the expense of variable oxygen content. We show that, though the average cobalt valence is the same for all the samples, the ferromagnetic state is dramatically extended from the narrow window 200–270 K for $EuBaCo_2O_{5.49}$ to the temperature range 10–320 K for the compounds $Eu_{1-x}Ca_xBaCo_2O_{5.50\pm\delta}$ ($x = 0.05$–$0.2$) without affecting the $T_{IM}$. We propose a scenario based on the existence of canted antiferromagnetic domains behaving as paramagnetic entities, where calcium doping induces ferromagnetic $Co^{3+}$–O–$Co^{4+}$ interactions through cobalt disproportionation according to the equation $2Co^{3+} \leftrightarrow Co^{4+} + Co^{2+}$. We explain the transport properties of these oxides on the basis of local hopping of electrons and holes between the cobalt ions in different oxidation states in the doped compositions.

## 2. Experimental details

The samples $Eu_{1-x}Ca_xBaCo_2O_{5.50\pm\delta}$ ($x = 0$, 0.05, 0.1 and 0.2) were synthesized from mixtures of oxides $Eu_2O_3$, $CaCO_3$, $BaCO_3$ and $Co_3O_4$ in stoichiometric ratio. $Eu_2O_3$ was dried at 900 °C prior to use and $BaCO_3$, $CaCO_3$ and $Co_3O_4$ used as-received. The appropriate proportions of the starting materials were weighed and thoroughly mixed by a mortar and pestle, adding ethanol for homogeneous mixing. The intimate mixtures was first heated in air at 1000 °C for 24 h. They were then ground and pressed in the form of bars and sintered in air at 1100 °C for 24 h and finally cooled down to room temperature at 100 °C $h^{-1}$. The x-ray diffraction (XRD) patterns above and below the metal–insulator transition were recorded using a Philips X'pertPro diffractometer with Cu K$\alpha$ radiation. The energy-dispersive spectroscopy (EDS) analysis performed with a Kevex analyzer mounted on a JEOL 200 CX electron microscope allowed the normal cationic composition to be confirmed. The oxygen content determined by iodometric titration in argon atmosphere allowed these samples to be formulated as $EuBaCo_2O_{5.49}$, $Eu_{0.95}Ca_{0.05}BaCo_2O_{5.48}$, $Eu_{0.9}Ca_{0.1}BaCo_2O_{5.44}$ and $Eu_{0.8}Ca_{0.2}BaCo_2O_{5.41}$, corresponding to average cobalt valences ($V_{Co}$) of +2.99, +3.00, +2.99 and +3.01, respectively.

The electrical transport and magnetoresistance at 7 T were measured by a standard four-probe method using a physical property measuring system (PPMS) within the temperature range of 5–400 K. The magnetic measurements were carried out with a SQUID magnetometer (MPMS, Quantum Design). For each sample the zero field cooled (ZFC) and field cooled (FC) data were collected with an applied field of 0.3 T. The magnetization versus applied field ($M$–$H$) measurements were performed with an applied field of ±5 T.

## 3. Results

The high temperature and room temperature XRD patterns of all the samples are better indexed with the orthorhombic structure with the space group *Pmmm*. The diffraction pattern was analyzed by the Fullprof suite software [26]. The details of the cell parameters at 450 K and at room temperature, respectively, above and below the $T_{IM}$ (∼340 K) are summarized in table 1. The cell parameters do not show significant change with calcium doping for all the compositions at room temperature as well as at higher temperatures. However, it shows that the *a*-axis becomes larger below $T_{IM}$, whereas *b*- and *c*-axes exhibit normal thermal behaviour for all the compositions. Such temperature dependent behaviour of the lattice parameters is associated with structural change across the metal–insulator transition [22].

**Table 1.** Structural parameters of $Eu_{1-x}Ca_xBaCo_2O_{5.50\pm\delta}$ above and below the metal–insulator transition.

| | $T < T_{IM}$ (room temperature) | | | | $T > T_{IM}$ (450 K) | | | |
|---|---|---|---|---|---|---|---|---|
| | S. G. ($Pmmm$) | | | | S. G. ($Pmmm$) | | | |
| $x$ | $a$ (Å) | $b$ (Å) | $c$ (Å) | $V$ (Å$^3$) | $a$ (Å) | $b$ (Å) | $c$ (Å) | $V$ (Å$^3$) |
| 0 | 3.8823(1) | 7.8187(2) | 7.5481(2) | 229.12(1) | 3.8701(1) | 7.8444(2) | 7.5762(2) | 230.00(1) |
| 0.05 | 3.8766(1) | 7.8244(2) | 7.5492(1) | 228.99(1) | 3.8669(1) | 7.8466(2) | 7.5777(1) | 229.92(1) |
| 0.1 | 3.8758(1) | 7.8354(2) | 7.5449(1) | 229.12(1) | 3.8642(1) | 7.8560(2) | 7.5722(2) | 229.87(1) |
| 0.2 | 3.8709(2) | 7.8336(3) | 7.5499(2) | 228.94(2) | 3.8649(1) | 7.8537(2) | 7.5735(1) | 229.88(1) |

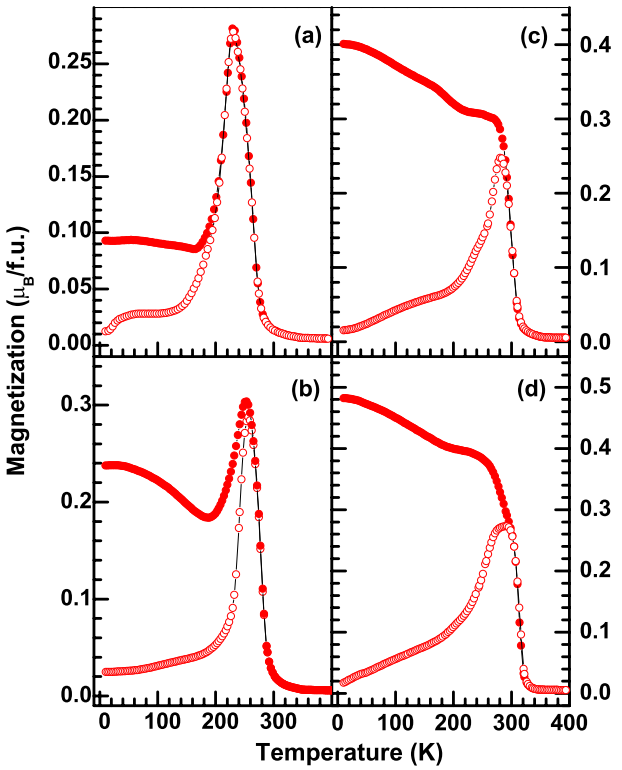


**Figure 2.** M(T) curves of $Eu_{1-x}Ca_xBaCo_2O_{5.50\pm\delta}$ registered at 0.3 T: (a) $EuBaCo_2O_{5.49}$, (b) $Eu_{0.95}Ca_{0.05}BaCo_2O_{5.48}$, (c) $Eu_{0.9}Ca_{0.1}BaCo_2O_{5.44}$ and (d) $Eu_{0.8}Ca_{0.2}BaCo_2O_{5.41}$. The open (solid) symbols correspond to ZFC (FC) data.

The zero field cooled (ZFC) and field cooled (FC) magnetization curves of the parent compound $EuBaCo_2O_{5.49}$ registered in an applied field of 0.3 T exhibit a magnetization peak centred at 200–280 K (figure 2(a)), indicative of successive magnetic transitions, as previously observed [15]. Thus the ferromagnetic state appears in a narrow temperature window of ∼70 K. The behaviour of the calcium substituted phases is significantly different from that of the parent compound. The Ca-substituted phases exhibit a much broader temperature window of the ferromagnetic state (figures 2(b)–(d)) and the ferromagnetic transition ($T_C$) shifts to higher temperature. The $T_C$ gradually increases with the increase in $x$, i.e. 290, 310 and 320 K for $x = 0.05$, 0.1 and 0.2, respectively (figures 2(b)–(d)). It is worth mentioning that though the ZFC data of the Ca-substituted compositions are qualitatively the same as those of the parent compound (figures 2(a)–(d)), the magnetization decreases sluggishly for $x = 0.1$ and 0.2 below the temperature where ZFC and FC data diverge (figures 2(c) and (d)). The FC magnetization data for $x = 0.1$ and 0.2 substitutions show a small downward kink immediately below $T_C$, followed by a monotonous increase, without any saturation till 10 K (figures 2(c) and (d)). One also observes a gradual increase of the low temperature magnetization values as $x$ increases (figures 2(a)–(d)). Thus, these results demonstrate that the substitution of calcium for europium in the '112' phase $EuBaCo_2O_{5.50}$ induces ferromagnetism in the whole temperature range from 10 to 320 K.

In order to check the magnetic ground state we have registered isothermal magnetization $M(H)$ curves at different temperatures. Only the $M(H)$ curves recorded at 10 and 300 K for all the compositions are shown in figure 3. For $x = 0$, the $M(H)$ curve at 10 K (figure 3(a)) shows typical behaviour of an antiferromagnetic material. Interestingly, for a small substitution of Eu by Ca ($x = 0.05$) the nature of the $M(H)$ curve at 10 K changes towards that of a ferromagnetic material. The compositions with $x = 0.1$ and 0.2 show a clear signature of ferromagnetism at 10 K (figure 3(a)). The magnetization value does not saturate even at a field as high as 5 T, but it increases significantly with $x$ (figure 3(a)). The $M(H)$ curves registered at 300 K (figure 3(b)) show that the $x = 0$ and 0.05 compositions remain paramagnetic at this temperature, whereas the $x = 0.1$ and 0.2 phases become ferromagnetic, but with a very small coercive field (figure 3(b)). The $M(H)$ measurements at other temperatures reveal that the parent compound shows a ferromagnetic behaviour only in a narrow window in the neighbourhood of 250 K, whereas the Ca-substituted compositions show a ferromagnetic behaviour in the whole temperature range below $T_C$ (data not shown). In all cases, the magnetization value at a given temperature and a maximum field increases as $x$ increases. For all the doped samples the coercive field decreases systematically with the increase in temperature.

The temperature dependent resistivity of $Eu_{1-x}Ca_xBaCo_2O_{5.50\pm\delta}$ (figure 4(a)) shows a sudden increase of the resistivity by about one order of magnitude around 345 K for all the compositions, the latter is associated with a metal–insulator transition characteristic of this family of compounds [1, 3]. Note that though the Ca-substitution drastically increases $T_C$ (figure 2), it does not significantly affect the metal–insulator transition temperature. The $T_{IM}$ region is enlarged in the inset of figure 4(a) for clarity of the transition temperature of all compositions. Below $T_{IM}$ the resistivity of the

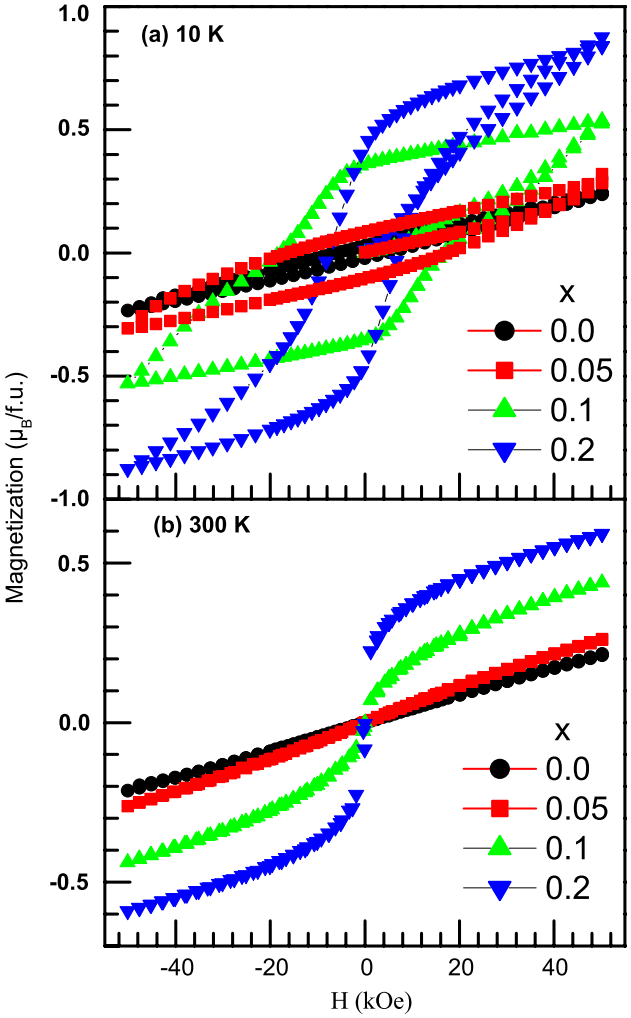


**Figure 3.** $M(H)$ curves of $Eu_{1-x}Ca_xBaCo_2O_{5.50\pm\delta}$ registered at: (a) 10 K and (b) 300 K.

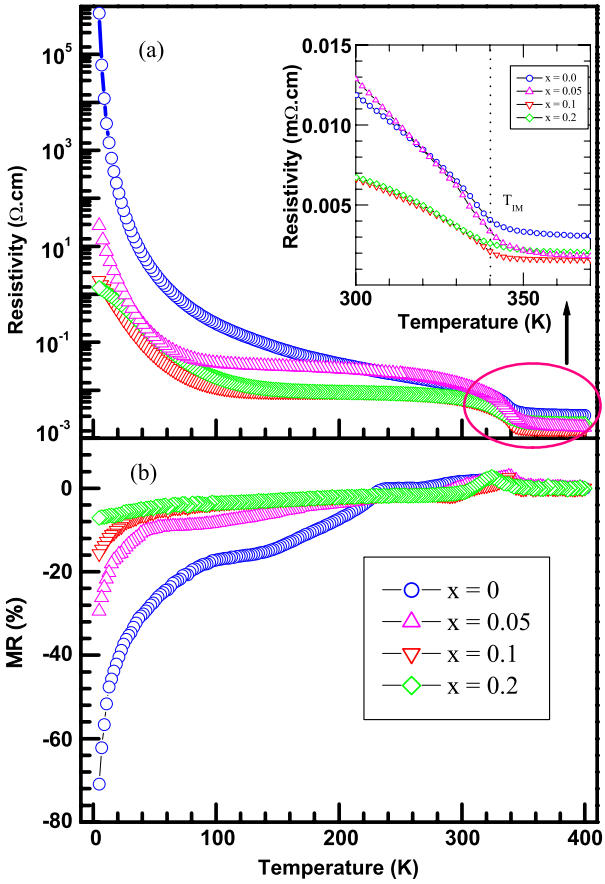


**Figure 4.** (a) Temperature dependent resistivity of $Eu_{1-x}Ca_xBaCo_2O_{5.50\pm\delta}$. The inset is the enlarged part of the metal–insulator transition region. (b) The variation of magnetoresistance with $x$ as a function of temperature.

parent composition is that of a semiconductor, as reported earlier [1, 3]. However, the Ca-doped samples differ from the parent oxide by the fact that the resistivity becomes much smaller and is temperature independent in a wide range of temperatures from $T_{IM}$ (∼340 K) to ∼100 K (figure 4(a)). Moreover, at very low temperature ($T < 10$ K) the resistivity drops by several orders of magnitude by Ca-doping, even for very small calcium contents, as shown for instance for the $x = 0.05$ sample which exhibits a resistivity $10^5$ smaller than that of the $x = 0$ sample at 5 K (figure 4(a)). The MR is calculated from the expression $MR(\%) = [\{\rho(7) - \rho(0)\}/\rho(0)] \times 100$, where $\rho(0)$ is the sample resistivity at 0 T and $\rho(7)$ in an applied field of 7 T are plotted in figure 4(b). The low temperature MR effect changes abruptly with the increase in $x$.

## 4. Discussion

These results show that the substitution of calcium for europium affects significantly the magnetic properties of the '112' cobaltites. One indeed observes an extension of the ferromagnetism down to 10 K and a linear increase of the Curie temperature, along with an increase of magnetization with respect to the magnetic field and temperature (figures 2 and 3) as $x$ increases. In contrast, no change of the metal–insulator transition temperature is observed (figure 4). Such a behaviour can neither be explained by size effects nor by the cobalt valency effect. $Ca^{2+}$ and $Eu^{3+}$ cations have indeed very close ionic radii, i.e. 1.18 Å and 1.12 Å, respectively [27], and consequently no significant change of the Co–O–Co bond angle can be expected. Similarly, the cobalt valency remains unchanged in the series. This is corroborated by the insignificant change of the structural parameters, as the calcium content varies.

In order to get insight into such magnetic and electrical properties, we have plotted $\chi^{-1}$ versus temperature in figure 5. One can see the change in slope of the $\chi^{-1}$ plot in the paramagnetic phase. It is clear from the plot that the change in slope with calcium doping below $T_{IM}$ is more drastic than above $T_{IM}$. The increase in slope signifies a decrease in effective moment from the Curie–Weiss law. The effective moment decreases with the increase in calcium doping and this decrease is more pronounced below $T_{IM}$. The effective moment above and below $T_{IM}$ obtained from the Curie–Weiss fitting is shown in table 2. It is very curious that with the calcium doping the effective moment decreases in the paramagnetic phase.

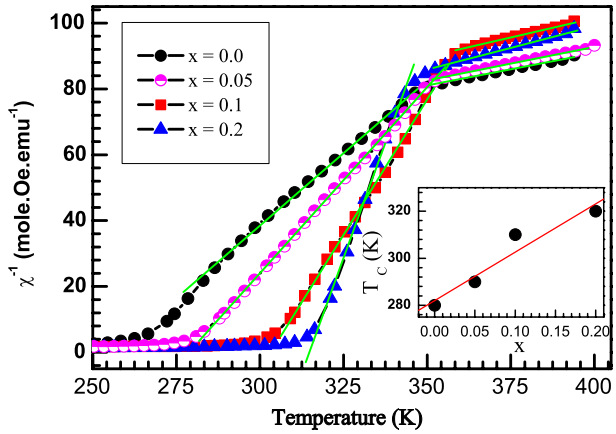


**Figure 5.** Inverse susceptibility, $\chi^{-1}$ plot as a function of temperature. The inset shows variation of $T_C$ with $x$ for $Eu_{1-x}Ca_xBaCo_2O_{5.50\pm\delta}$.

**Table 2.** Calculated effective moment and Weiss temperature from the Curie–Weiss law for $Eu_{1-x}Ca_xBaCo_2O_{5.50\pm\delta}$ above and below the metal–insulator transition.

| | $T < T_{IM}$ | | $T > T_{IM}$ | |
|---|---|---|---|---|
| $x$ | $\mu_{eff}$ ($\mu_B$) | $\Theta_P$ (K) | $\mu_{eff}$ ($\mu_B$) | $\Theta_P$ (K) |
| 0 | 3.03 | 256 | 6.40 | −61.85 |
| 0.05 | 2.672 | 278 | 6.30 | −56.48 |
| 0.1 | 2.22 | 303 | 5.85 | −30.12 |
| 0.2 | 1.70 | 315 | 5.54 | 22.73 |

Though the decrease in moment is less above $T_{IM}$, 6.30 $\mu_B$/f.u. for $x = 0-5.54$ $\mu_B$/f.u. for $x = 0.2$, it becomes drastic below $T_{IM}$ i.e. 3.03 $\mu_B$/f.u. for $x = 0-1.7$ $\mu_B$/f.u. for $x = 0.2$. This decrease of effective moment as $x$ increases, above and below $T_{IM}$, where the cobalt valency remains equal to +3, cannot be explained by the spin-state transition of $Co^{3+}$ that was previously proposed by several authors [1, 4, 5]. Thus it is most likely that the metal–insulator transition, which corresponds to a structural transition does not involve any spin-state transition, in agreement with the experimental and theoretical studies performed recently [21–25].

Now we propose a different scenario in order to explain such a complex magnetic behaviour. The observed moment in the paramagnetic state does not correspond to the spins of individual $Co^{3+}$ ions, but rather to a group of cations called 'domains'. Within the domains cobalt spins are arranged in a canted antiferromagntic fashion which gives an effective $S$ ($S_{eff}$) corresponding to the observed moment. Such $S_{eff}$ was considered in ordered to explain the higher moment in the manganite system [28, 29]. In a competing paramagnetic, ferromagnetic and antiferromagnetic environment the canted magnetic structure is not unusual [5, 6, 24]. These domains act as paramagnets, with an effective antiferromagnetic coupling with each other above the $T_{IM}$. Below $T_{IM}$ the cobalt spin state remains unchanged, only the canting angle between the spins of the domains is modified due to the structural change. Such a structural transition may reduce the canting angle and hence the moment in the insulating phase. A rather similar mechanism was described for half-doped manganites [30]. However, these moments are ferromagnetically coupled giving a positive Weiss temperature (table 2) below $T_{IM}$. On further lowering the temperature they align ferromagnetically, with a sudden jump in magnetization followed by a decrease in magnetization, signifying an antiferromagnetic transition. Thus the ferromagnetic state corresponds to an entropy driven ground state within an antiferromagnetic matrix.

Let us now discuss the effect of calcium doping, and especially the decrease of the effective moment as the calcium content increases. Only a small content of oxygen (less than 2% for $x = 0.2$) is removed from the structure as calcium is introduced, leaving the cobalt valency +3. The small oxygen deficiency with respect to '$O_{5.5}$', that converts cobalt octahedra into pyramids, also cannot account for the decrease of the effective moment. In contrast, divalent calcium, sitting on the trivalent europium sites, may locally change the crystal field and favour a partial and local disproportionation of trivalent cobalt according to the equation $2Co^{3+} \leftrightarrow Co^{4+} + Co^{2+}$. In this scenario, $Co^{4+}$ will sit preferentially in the octahedra with an IS state ($S = 3/2$), whereas $Co^{2+}$ will go to pyramids keeping an HS state ($S = 3/2$). Such a disproportionation qualitatively explains the 14% reduction of effective moment for 20% calcium doping. One must indeed keep in mind that as soon as $Co^{4+}$ ions are introduced in the system, they contribute to $Co^{3+}$–O–$Co^{4+}$, ferromagnetic superexchange interactions, whereas HS $Co^{3+}$ and HS $Co^{2+}$ will form $Co^{2+}$–O–$Co^{3+}$ antiferromagnetic interactions [31]. Consequently, the mode of coupling in the paramagnetic phase changes from antiferromagnetic for $x = 0$ to ferromagnetic for $x = 0.2$ above $T_{IM}$ (see table 2).

The change in slope of the $\chi^{-1}$ plot below $T_{IM}$ causes about 40% changes in effective moment for $x = 0.2$. To account for this large change in slope, one has to consider the strongly enhanced ferromagnetic coupling between the domains discussed above. This is reflected by the increase in $T_C$ with $x$ (see inset of figure 5). Such an enhancement in ferromagnetic coupling in the paramagnetic phase and of $T_C$ originates from the increase of ferromagnetic $Co^{3+}$–O–$Co^{4+}$ interaction within the domains, as $x$ increases. One can consider that calcium doping assists the formation of ferromagnetic droplets within the competing paramagnetic–ferromagnetic–antiferromagnetic matrix. These ferromagnetic components persist till the lowest temperature. Thus the ferromagnetic component increases with the calcium content, which is consistent with our observation. The divergence of ZFC from the FC curve and a large thermomagnetic hysteresis loop below $T_C$ indicate the existence of phase separation, i.e. the presence of independent ferromagnetic regions in an antiferromagnetic matrix. The occurrence of phase separation in similar Gd systems has been reported by Taskin *et al* [6]. Moreover, the increase of the moment as the temperature decreases could be an indication of the growth of the ferromagnetic phase at the expense of the antiferromagnetic phase (figure 2).

The lack of saturation of the magnetization in the $M(H)$ curve even at a field of 5 T suggests that the antiferromagnetic component transforms to the ferromagnetic one with increasing field (figure 3). The large coercive field

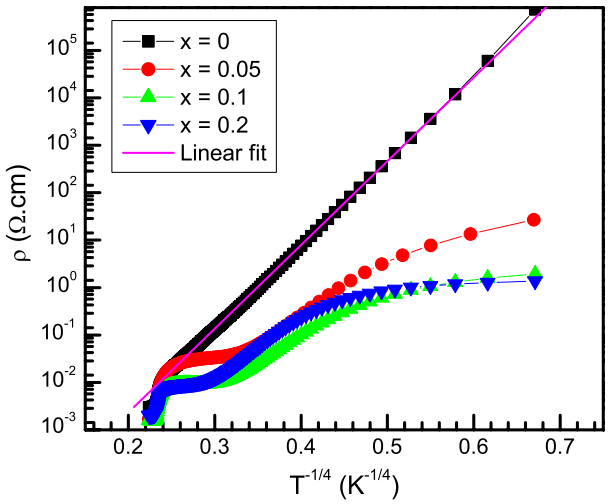


**Figure 6.** The $T^{-1/4}$ dependence of resistivity $\rho$ of $Eu_{1-x}Ca_xBaCo_2O_{5.50\pm\delta}$ compositions.

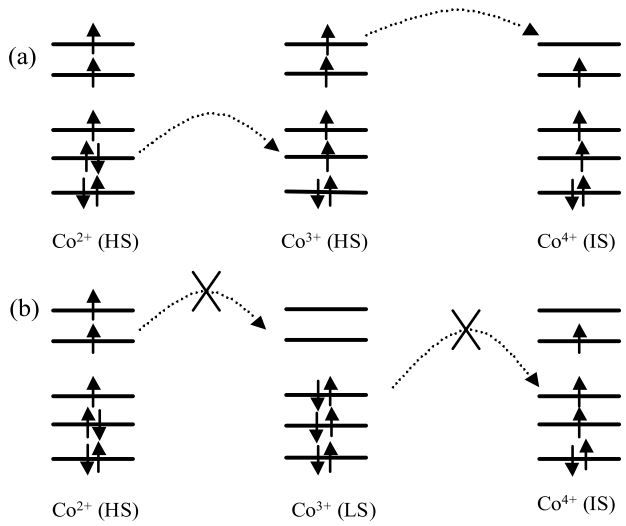


**Figure 7.** (a) Schematic diagram of possible electron and hole hopping between the HS $Co^{3+}$, HS $Co^{2+}$ and IS $Co^{4+}$, and (b) between the LS $Co^{3+}$, HS $Co^{2+}$ and IS $Co^{4+}$.

for $x = 0.1$, compared to the $x = 0.2$ composition (figure 3) could be due to a larger disorder of the ferromagnetic domain for $x = 0.1$.

Since the metal–insulator transition is associated with the structural transition, the structural similarity and the comparable structural parameters (table 1) of all the compositions could be at the origin of the same metal–insulator transition temperature. Moreover, the change in resistivity with calcium doping can be understood on the basis of cobalt disproportionation. The transport properties of the parent composition follow the variable range hopping behaviour (linear fit in figure 6). In contrast, for small calcium doping, one does not observe the same law (figure 6). In the parent compound the conventional semiconducting transport occurs, due to the mobility of the thermally excited hole and electron corresponding to the $Co^{4+}$ and $Co^{2+}$ species, deriving from ground state $Co^{3+}$ ions. Then, calcium doping causes the formation of $Co^{4+}$ and $Co^{2+}$ which can easily transfer the corresponding hole and electron to the neighbouring HS $Co^{3+}$ ion as shown schematically in figure 7(a). In contrast, the transfer of the hole and the electron from the neighbouring $Co^{4+}$ and $Co^{2+}$, respectively, to LS $Co^{3+}$ ions is spin forbidden (figure 7(b)). Such hopping of electrons and holes brings local spin polarization. Such an already spin polarized state could be responsible for a lower MR effect with the increase in $x$ (figure 4(b)). Thus the IS $Co^{4+}$, HS $Co^{3+}$ and $Co^{2+}$ can qualitatively explain the drops in resistivity by calcium doping.

## 5. Conclusion

In conclusion, the substitution of calcium for europium in the '112' cobaltite, $EuBaCo_2O_{5.5}$ expands drastically the ferromagnetism in this phase in the whole temperature range from 10 to 320 K with increasing $T_C$, but does not affect the metal–insulator transition temperature $T_{IM}$. These results suggest that $T_{IM}$ is driven by the structural transition and is not related to any spin-state transition. Considering the spectacular variation of the effective moment at $T_{IM}$ with Ca-content, we propose a phase separation scenario, involving the formation of canted antiferromagnetic domains in the paramagnetic phase, whose behaviour is dramatically modified by calcium doping. The latter indeed turns the crystal field energy and facilitates the disproportionation of $Co^{3+}$ into $Co^{2+}$ and $Co^{4+}$, enhancing ferromagnetism, due to the $Co^{3+}$–O–$Co^{4+}$ superexchange interactions. Further investigations by neutron diffraction and theoretical studies will be required to understand the origin of such a complex magnetic behaviour in this system.

## Acknowledgment

The authors thank Dr M B Lepetit for helpful discussions.

## References

[1] Martin C, Maignan A, Pelloquin D, Nguyen N and Raveau B 1997 *Appl. Phys. Lett.* **71** 1421
[2] Troyanchuk I O, Kasper N V, Khalyavin D D, Szymczak H, Szymczak R and Baran M 1998 *Phys. Rev. Lett.* **80** 3380
[3] Maignan A, Martin C, Pelloquin D, Nguyen N and Raveau B 1999 *J. Solid State Chem.* **142** 247
[4] Respaud M, Frontera C, García-Muñoz J L, Aranda M A G, Raquet B, Broto J M, Rakoto H, Goiran M, Llobet A and Rodríguez-Carvajal J 2001 *Phys. Rev.* B **64** 214401
[5] Taskin A A, Lavrov A N and Ando Y 2003 *Phys. Rev. Lett.* **90** 227201
[6] Taskin A A, Lavrov A N and Ando Y 2005 *Phys. Rev.* B **71** 134414
[7] Zhou Z X and Schlottmann P 2005 *Phys. Rev.* B **71** 174401
[8] Baran M, Gatalskaya V I, Szymczak R, Shiryaev S V, Barilo S N, Bychkov G L and Szymczak H 2005 *J. Phys.: Condens. Matter* **17** 5613
[9] Khalyavin D D, Barilo S N, Shiryaev S V, Bychkov G L, Troyanchuk I O, Furrer A, Allenspach P, Szymczak H and Szymczak R 2003 *Phys. Rev.* B **67** 214421
[10] Soda M, Yasui Y, Fujita T, Miyashita T, Sato M and Kakurai K 2003 *J. Phys. Soc. Japan* **72** 1729
[11] Soda M, Yasui Y, Ito M, Iikubo S, Sato M and Kakurai K 2004 *J. Phys. Soc. Japan* **73** 464

[12] Chernenkov Y P, Plakhty V P, Fedorov V I, Barilo S N, Shiryaev S V and Bychkov G L 2005 *Phys. Rev.* B **71** 184105
[13] Maignan A, Caignaert V, Raveau B, Khomskii D and Sawatzky G 2004 *Phys. Rev. Lett.* **93** 26401
[14] Zhou H D and Goodenough J B 2004 *J. Solid State Chem.* **177** 3339
[15] Roy S, Dubenko I S, Khan M, Condon E M, Craig J, Ali N, Liu W and Mitchell B S 2005 *Phys. Rev.* B **71** 024419
[16] Moritomo Y, Akimoto T, Takeo M, Machida A, Nishibori E, Takata M, Sakata M, Ohoyama K and Nakamura A 2000 *Phys. Rev.* B **61** R13325
[17] Burley J C, Mitchell J F, Short S, Miller D and Tang Y 2003 *J. Solid State Chem.* **170** 339
[18] Plakhty V P, Chernenkov Y P, Barilo S N, Podlesnyak A, Pomjakushina E, Moskvin E V and Gavrilov S V 2005 *Phys. Rev.* B **71** 214407
[19] Roy S, Khan M, Guo Y Q, Craig J and Ali N 2002 *Phys. Rev.* B **65** 64437
[20] Kim W S, Chi E O, Choi H S, Hur N H, Oh S-J and Ri H-C 2000 *Solid State Commun.* **116** 609
[21] Flawell W R, Thomas A G, Tsoutsou D, Mallick A K, North M, Seddon E A, Cacho C, Malins A E R, Patel S, Stockbauer R L, Kurtz R L, Sprunger P T, Barilo S N, Shiryaev S V and Bychkov G L 2004 *Phys. Rev.* B **70** 224427
[22] Conder K, Pomjakushina E, Pomjakustin V, Stingaciu M, Streule S and Podlesnyak A 2005 *J. Phys.: Condens. Matter* **17** 5813
[23] Wu H 2001 *Phys. Rev.* B **64** 92413
[24] Wu H 2003 *J. Phys.: Condens. Matter* **15** 503
[25] Hidaka M, Soejima M, Wijesundera R P, Soda M, Sato M, Choi S-H, Sung N E, Kim M G and Lee J M 2006 *Phys. Status Solidi* b **243** 1813
[26] Rodriguez-Carvajal J 1990 *Abstracts of the Satellite Mtg on Powder Diffraction of the XV Congr. of the IUCr (Toulouse)* p 127
[27] Shannon R D 1976 *Acta Crystallogr.* A **32** 751
[28] Gayathri N, Raychaudhuri A K, Tiwary S K, Gundakaram R, Arulraj A and Rao C N R 1997 *Phys. Rev.* B **56** 1345
[29] Tanaka J, Nozaki H, Horiuchet S and Tsukioka M 1983 *J. Phys. Lett.* **44** L129
[30] Daoud-Aladine A, Rodríguez-Carvajal J, Pinsard-Gaudart L, Fernández-Díaz M T and Revcolevschi A 2002 *Phys. Rev. Lett.* **89** 97205
[31] Goodenough J B 1963 *Magnetism and the Chemical Bond* (New York: Wiley)